Structural Features of Target RNA Molecules Greatly Modulate the Cleavage Efficiency of *trans*-Acting Delta Ribozymes†

Agata Świątkowska, Mariola Dutkiewicz, and Jerzy Ciesiołka*

Institute of Bioorganic Chemistry, Polish Academy of Sciences, Poznań 61-704, Poland

Received November 23, 2006; Revised Manuscript Received February 6, 2007

ABSTRACT: The aim of this work was to shed some more light on factors influencing the effectiveness of delta ribozyme cleavage of structured RNA molecules. An oligoribonucleotide that corresponds to the 3′-terminal region X of HCV RNA and yeast $tRNA^{Phe}$ were used as representative RNA targets. Only a few sites susceptible to ribozyme cleavage were identified in these targets using a combinatorial library of ribozyme variants, in which the region responsible for ribozyme−target interaction was randomized. On the other hand, the targets were fairly accessible for binding of complementary oligonucleotides, as was shown by 6-mer DNA libraries and RNase H approach. Moreover, the specifically acting ribozymes cleaved the targets precisely but with unexpectedly modest efficacy. To explain these observations, six model RNA molecules were designed, in which the same seven nucleotide long sequence recognized by the delta ribozyme was always single stranded but was embedded into different RNA structural context. These molecules were cleaved with differentiated rates, and the corresponding k_2 values were in the range of 0.91−0.021 min^{-1}; thus they differed almost 50-fold. This clearly shows that cleavage of structured RNAs might be much slower than cleavage of a short unstructured oligoribonucleotide, despite full accessibility of the targeted regions for hybridization. Restricted possibilities of conformational transitions, which are necessary to occur on the cleavage reaction trajectory, seem to be responsible for these differences. Their magnitude, which was evaluated in this work, should be taken into account while considering the use of delta ribozymes for practical applications.

Among all known ribozymes, delta ribozymes have some unique characteristics, which make them very attractive as *trans*-acting molecular tools in the regulation of gene expression and in biochemical applications (*1*−*3*). These ribozymes are the first catalytic RNA molecules found naturally occurring in human cells. The very compact spatial structure makes them unusually stable in the intracellular environment. A half-life of over 100 h has been estimated for the antigenomic ribozyme variant (*4*). The ribozymes are catalytically active at low Mg^{2+} ion concentration approaching physiological conditions, and the substrate−ribozyme recognition element (helix P1 in Figure 1) consists of only seven base pairs facilitating ribozyme turnover. To date, delta ribozymes have been employed to attack RNAs encoding the delta antigen (*5*), HBV[1] pregenome (*6*), subtilase-like pro-protein convertase (*7*), uracil phosphoribosyltransferase (*8*, *9*), hypoxanthine−xanthine−guanine phosphoribosyltransferase (*9*), chimeric BCR-ABL-luciferase (*10*), EF-Tu (*11*), and 5′UTR HCV (*12*). Delta ribozymes have also been used as molecular scissors for the purpose of correct processing of the 3′ ends of RNA transcripts obtained in vitro with T7 RNA polymerase. This can be accomplished with the ribozymes acting either in their *cis* (*13*) or *trans* forms (*14*). Although the fascinating discovery of interfering RNAs has dominated the experimental approaches of silencing of gene expression, more recent data have pointed out some drawbacks of this new technology (*15*, *16*). Therefore, in some particular cases antisense oligonucleotides and ribozymes might still be applied as alternative tools in the functional genomics and nucleic acid-based therapy.

In a majority of gene silencing experiments with the use of ribozymes or other oligonucleotide tools, the coding regions of target RNA molecules have been attacked. However, the idea to attack the noncoding regions of RNA is very attractive, and sometimes it seems to be the most appropriate. In the case of RNA viruses, which undergo very fast changes, only their highly conservative sequences can be targeted effectively. Although some coding regions are also conservative, they cannot be efficiently cleaved in vivo due to the occurrence of the "virus escape effect" which has been observed for fast and slow replicating viruses (*17*−*20*). Unfortunately, attacking the noncoding regions is experimentally difficult. Such regions are usually highly structured and, in consequence, rather inaccessible for hybridization. Moreover, earlier reports have suggested that some other factors besides RNA accessibility may limit the efficiency of RNA targeting by ribozymes (*6*). Revealing such effects is crucial for the effective use of ribozymes as biomedical and biochemical nucleic acid-based tools.

The aim of the present work is to shed some more light on factors that limit the effectiveness of delta ribozyme

† This work was supported by the Polish Ministry of Science and Higher Education (Grant 2P04A05128 to J.C.).

* To whom correspondence should be addressed. Tel: +48 61 8528503. Fax: +48 61 8520532. E-mail: ciesiolk@ibch.poznan.pl.

[1] Abbreviations: HBV, hepatitis B virus; HCV, hepatitis C virus; Py, pyrimidine nucleoside; RT, reverse transcription; UTR, untranslated region; HPLC, high-pressure liquid chromatography.

10.1021/bi6024287 CCC: $37.00
Published on Web 04/11/2007

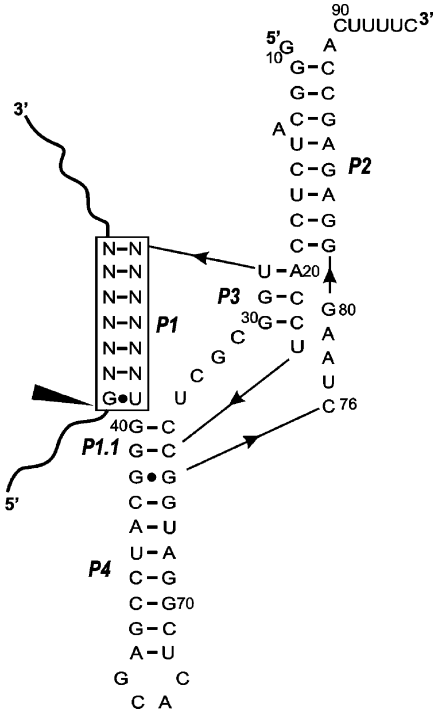

FIGURE 1: Combinatorial library of *trans*-acting variants of the antigenomic delta ribozyme. The randomized regions are boxed. Numbering of nucleotides corresponds to the wild-type ribozyme sequence, and base-paired segments are denoted P1 to P4. The catalytic cleavage site is marked by the filled triangle.

cleavage. Specifically, we report how the different structural context, in which targeted sequences are embedded in RNA molecules, may influence cleavage efficacy. As the model structured RNA, we used an oligoribonucleotide which corresponds to the 3′-terminal noncoding region X of viral HCV RNA. Its secondary structure has been recently studied in our laboratory (*21*). Yeast $tRNA^{Phe}$ was also employed as a representative of highly structured RNAs. It turned out that these RNA targets were hardly susceptible to ribozyme cleavage despite their much better accessibility for binding of complementary oligonucleotides. In order to reveal the influence of RNA higher order structure on ribozyme catalysis, we performed a kinetic analysis of cleavage reactions of specifically designed model RNA substrates. In these substrates the same seven nucleotide long stretch recognized by the wild-type delta ribozyme was always single stranded, but it was embedded into different RNA structural contexts.

EXPERIMENTAL PROCEDURES

Materials. The chemicals were purchased from Fluka or Sigma, and the enzymes were supplied by MBI Fermentas. [γ-^{32}P]ATP (5000 Ci/mmol) was from ICN. The oligoribonucleotides (TS) 5′-CUUUCCUCUUCGGGUCGGCA-3′ and (SL2a/SL2b) 5′-AGUCACGGCUAGCUGUGAAAGGUCCGUGAGCCG-3′ were purchased from Dharmacon (Lafayette, CO). Oligodeoxyribonucleotides were synthesized by the DNA Sequencing and Oligonucleotide Service of the Institute of Biochemistry and Biophysics PAN, Warsaw. Yeast $tRNA^{Phe}$ of specific phenylalanine acceptance 1200−1400 pmol/A_{260} unit was prepared from crude baker's yeast tRNA by standard column chromatography procedures including benzoylated DEAE-cellulose and Sepharose-4B (Pharmacia, Sweden). Final purification was done by HPLC on a TSK-gel DEAE 2SW column (Toyo Soda, Japan).

DNA Templates for the Ribozyme Combinatorial Library and Specific Ribozyme Variants. The transcription template for the wild *trans*-acting delta ribozyme was prepared as described previously (*22*). Briefly, two oligomers were synthesized, (RA) 5′-*TAATACGACTCACTATA*GGGCATCTCCACC-3′and (RW) 5′-GAAAAGTGGCTCTCCCTTAGCCATCCGAGTGCTCGGATGCCCA(GGTCGG)ACCGCGAGGAGGTGGAGATGCCC-3′ (letters in italics mark the T7 RNA polymerase promoter; complementary sequences are underlined; letters in parentheses denote nucleotides engaged in the formation of the P1 helix). For delta ribozyme combinatorial library and specific ribozyme variants additional oligomers were synthesized, in which the six nucleotide long stretch that is shown in parentheses in the RW oligomer was replaced as follows: (RL) 5′-NNNNNN-3′, (R35) 5′-TGAAAG-3′, and (R46) 5′-TGAGCC-3′. The oligomers RA and RW (or derivatives of the latter with changes in the P1 region) were annealed, and double-stranded DNA templates were generated by PCR. The reaction mixtures contained 1 μM both DNA oligomers, 75 mM Tris-HCl, pH 8.8, 20 mM $(NH_4)SO_4$, 0.01% Tween 20, 2 mM $MgCl_2$, 200 μM each dNTP, and 25 units/mL Taq polymerase. The reactions were performed on a Biometra UNO II thermocycler for eight cycles: 2 min at 94 °C, 30 s at 94 °C, 30 s at 46 °C, 2 min at 72 °C, and 5 min at 72 °C. The DNA was recovered by phenol/chloroform extraction, ethanol precipitated, and dissolved in TE buffer. For the catalytically inactive ribozyme variant with mutation C76G two DNA oligomers were synthesized: (T7) 5′-*TAATACGACTCACTATA*G-3′ and (R76G) 5′-GAAAAGTGGCTCTCCCTTACCCATC-3′ (the mutated nucleotide is underlined). Double-stranded DNA was generated in two steps by RT-PCR. In the first step cDNA was synthesized using the R76G primer and wild-type ribozyme as a template. Subsequently, RNA was digested with RNase A, and the cDNA was amplified by PCR.

DNA Templates for RNA Substrates. The dsDNA encoding yeast $tRNA^{Phe}$ was generated by PCR using two oligomers (*14*): (PHE76) 5′-TGGTGCGAATTCTGTGGATCGAACACAGGACCTCCAGATCTTCAGTCTGGCGCTCTCCCAACTGAGCTAAATCCGC-3′and (PHE36) 5′-*TAATACGACTCACTATA*GCGGATTTAGCTCAGTTGG-3′. The DNA template for transcription of RNA X(+) was prepared as described previously (*21*) using two oligomers: (X71) 5′-*TAATACGACTCACTATA*GGTGGCTCCATCTTAGCCCTAGTCACGGCTAGCTGTGAAAGGTCCGTGAGCCGC-3′ and (X58) 5′-ACATGATCTGCAGAGAGGCCAGTATCAGCACTCTCTGCAGTCATGCGGCTCACGGACC-3′. The PCR reactions were performed as described above. For RNA substrates TH3, TH5, TLM, TL5, and TL3 the following ten oligomers were synthesized: (TH3A) 5′-CCGACCCGCATGACTGCAGTATCGCAGTCA-3′, (TH3B) 5′-*TAATACGACTCACTATA*GCATGACTGCGATACTGC-3′, (TH5A) 5′-CTGTGACTGCAGTATCGCAGTCA-3′, (TH5B) 5′-*TAATACGACTCACTATA*GTCGGGTCGGCTGTGACTGCGATACTGC-3′, (TLMA) 5′-ATCGCAGTCATGCTTTTCCGACCCGTTTGCA-3′, (TLMB) 5′-*TAATACGACTCACTATA*GGGCAGTCATGCAAACGGGTCGGAAAAGCA-3′, (TL5A) 5′-ATCGCAGTCATGCCCGACCCGTTTTTTTGCA-3′, (TL5B) 5′-*TAATACGACTCACTATA*GGG-

CAGTCATGCAAAAAAACGGGTCGGGCA-3′, (TL3A) 5′-ATCGCAGTCATGCTTTTTTTTCCGACCCGCA-3′, and (TL3B) 5′-*TAATACGACTCACTATA*GGGCAGTCATGCGGGGTCGGAAAAAAAAGCA-3′. For each DNA template two appropriate oligomers (TH3A, TH3B; TH5A, TH5B; TLMA, TLMB; TL5A, TL5B; and TL3A, TL3B) were annealed, and dsDNA was generated by PCR. For the TH3 and TH5 substrates PCR reactions were performed in the same condition as for the wild-type ribozyme. For the TLM, TL5, and TL3 substrates the temperature of the annealing step was 64 °C. In the case of substrate SL1/SL2a two oligomers were used: (SL12A) 5′-ACATGATCTGCAGAGAGGCCAGTATCAGCACTCTCTGC-3′ and (SL12B) 5′-*TAATACGACTCACTATA*GGTCCGTGAGCCGCATGACTGCAGAGAGTGCTGATACTGGC-3′. The dsDNA template was obtained by PCR in the following conditions: 2 min at 94 °C, 30 s at 94 °C, 30 s at 62 °C, 2 min at 72 °C, and 5 min at 72 °C for eight cycles.

RNA in Vitro Transcription. The transcription reactions were carried out in a final volume of 50 μL containing 0.4 μM dsDNA template, 40 mM Tris-HCl, pH 8.0, 10 mM $MgCl_2$, 2 mM spermidine, 5 mM DTT, 1 mM each NTP, 0.01% Triton X-1000, 4 mM guanosine, and 2000 units/mL T7 RNA polymerase. The transcription mixture was incubated at 37 °C for 4 h. The transcription products were ethanol precipitated and purified by electrophoresis on an 8% polyacrylamide gel containing 8.3 M urea. The band corresponding to the RNA was visualized under UV light and cut out, and RNA was eluted from the gel with 0.3 M sodium acetate, pH 5.7, and 1 mM EDTA, ethanol precipitated, and dissolved in sterile water containing 0.1 mM EDTA. Purified RNA transcripts were labeled with ^{32}P at their 5′ ends by incubation with [γ-^{32}P]ATP and T4 polynucleotide kinase according to standard procedures.

Ribozyme Cleavage Reactions and Kinetic Analyses. The 5′-^{32}P-end-labeled RNA substrate (~1−10 nM) was mixed with the unlabeled delta ribozyme library (1−3 μM) or with specific ribozyme variants (~500−1000 nM) and subjected to a denaturation−renaturation procedure in the buffer containing 50 mM Tris-HCl, pH 7.5, and 0.1 mM EDTA, incubated for 2 min at 100 °C, chilled on ice for 10 min, and finally incubated for 10 min at 37 °C. The reaction was initiated by adding magnesium chloride solution to the final concentration of 10 mM and proceeded at 37 °C. Aliquots of the reaction mixture (5 μL) were removed at specified time points and quenched with equal volumes of 20 mM EDTA and 7 M urea. The reaction products were analyzed by electrophoresis on 12% polyacrylamide gels containing 8.3 M urea, visualized by autoradiography, or quantified using phosphorimaging screens and a Typhoon 8600 Imager with ImageQuant software (Molecular Dynamics).

The observed rate constant (k_{obs}) was obtained from data fitted to a single exponential equation: $[P]_t = [EP](1 - e^{-k_{obs}t})$, where k_{obs} is the first-order rate constant and $[P]_t$ and [EP] are the fraction cleaved at time t and the reaction end point, respectively (*39*). The maximum first-order cleavage rate constant (k_2) and the concentration at which the cleavage rate is half-maximal (K_M) were obtained from a plot of k_{obs} versus various concentrations of the ribozyme (15−1000 nM) and the Michaelis−Menten equation: $k_{obs} = k_2[E]_{tot}/K_M + [E]_{tot}$. The kinetic parameters were calculated using Microcal Origin 6.0 software. At least two independent experiments were performed for each measurement.

Mapping of RNA Accessibility to Hybridization with DNA 6-mer Libraries and RNase H Digestion. Prior to digestion with *Escherichia coli* RNase H (MBI Fermentas) the 5′-^{32}P-labeled RNA was renatured in the buffer 40 mM Tris-HCl, pH 8.0, 40 mM KCl, 10 mM $MgCl_2$, 1 mM DTT, and 0.1 mM EDTA by heating at 65 °C for 2 min and slow cooling to 37 °C. Subsequently, RNase H was added to the final concentration of 250 units/mL. The cleavage reactions were initiated by adding separately four DNA 6-mer libraries (final concentration of 200 μM) to four RNA samples (20000 cpm, 0.1−0.2 pmol of RNA in 10 μL reaction volume). The mixtures were incubated at 37 °C for 10 or 30 min. The reactions were quenched with equal volumes of a 20 mM EDTA/7 M urea mixture and frozen on dry ice. The digestion products were analyzed by electrophoresis on 12% polyacrylamide/8.3 M urea gels. Autoradiography was performed at −70 °C with an intensifying screen.

Determination of RNA Cleavage Sites. Products of ribozyme cleavage or RNase H digestion reactions were run on polyacrylamide gels along with the products of alkaline RNA hydrolysis and limited T1 ribonuclease (Pharmacia) digestion of the same RNA. An alkaline hydrolysis ladder was generated by incubation of the 5′-^{32}P-labeled RNA (dissolved in water) with formamide/3 mM $MgCl_2$ (1:5 v/v) at 100 °C for 10 min. Limited T1 digestion was performed in 50 mM sodium citrate, pH 5.3, and 7 M urea with 0.1 unit of the enzyme at 55 °C for 10 min.

Analysis of Ribozyme−Substrate Complexes on Nondenaturing Polyacrylamide Gels. The 5′-^{32}P-end-labeled RNA substrates (~1−10 nM) were mixed with a 100-fold excess of unlabeled inactive ribozyme variant C76G in the buffer containing 50 mM Tris-HCl, pH 7.5, and 0.1 mM EDTA, incubated for 2 min at 100 °C, chilled on ice, and incubated for 10 min at 37 °C. Magnesium chloride solution was added to a concentration of 10 mM, and the reaction mixtures (5 μL) were incubated for 5 min at 37 °C and subsequently were loaded on nondenaturing polyacrylamide gels. The gels contained 10% acrylamide−bisacrylamide (29:1), 40 mM Tris-HCl, pH 8.0, 40 mM KCl, 2.5 mM $MgCl_2$, and 0.1 mM EDTA. The running buffer contained 40 mM Tris-HCl, pH 8.0, and 2.5 mM $MgCl_2$. Electrophoresis was carried out at 40 mA. The gels were analyzed using phosphorimaging screens and the Typhoon 8600 Imager with ImageQuant software (Molecular Dynamics).

RESULTS

Searching for RNA Sites Accessible for Ribozyme Cleavage and Oligonucleotide Hybridization. To search for sites accessible for ribozyme cleavage on the studied structured RNAs, the combinatorial library of delta ribozyme variants was used (*5*; Figure 1). In the library the ribozyme's recognition sequence was randomized excluding the 3′-terminal uridine residue, which forms the G-U wobble base pair at the bottom of the recognition segment. It has been shown that other base pairs in this position are highly detrimental for cleavage in the wild-type ribozyme (*23*). Since the randomized P1 region consisted of six nucleotides, there were 4096 possible ribozyme variants in the library. For cleavage mapping the library was used at 1 μM

concentration; thus each ribozyme variant was present at the concentration of ca. 0.2 nM. The cleavage activity of the library was assayed using oligoribonucleotide 5′-CU-UCGGGUCGG-3′ with the seven nucleotide long sequence (underlined) corresponding to the substrate strand of the wild-type ribozyme. The oligomer was used at 2 nM concentration, and the reaction was performed at 37 °C in the presence of 10 mM Mg^{2+} ions (data not shown). The oligomer was cleaved with the observed rate constant k_{obs} of 0.019 min^{-1}. The cleavage extent exceeded 70% after 3 h, showing that the library was catalytically active and that the wild-type ribozyme variant present in the library was able to act with multiple turnover (ca. six ribozyme turnovers were estimated).

The delta ribozyme library was used for mapping RNA sites accessible for directed cleavage on two highly structured RNA molecules: X(+) RNA and yeast $tRNA^{Phe}$. Following incubation of the 5′-^{32}P-end-labeled X(+) RNA with the ribozyme library RL a few very faint bands were detected on the autoradiogram at U14, U34, C45, and U70 (Figure 2A, the autoradiogram on the left; in the case of two other autoradiograms site-specific ribozymes R35 and R46 were used, and these results are discussed later). The bands at U14 and U70 occurred, most likely, as a result of RNA self-degradation at labile UA phosphodiester bonds since these bands appeared also on other gels with no ribozyme library used (Figure 2A, two autoradiograms on the right). The bands at U34 and C45 correspond to binding of ribozyme variants to seven nucleotide long stretches: 35-GUGAAAG-41 and 46-GUGAGCC-52, which are located in the central part of the sequence (Figure 2A). Both stretches begin with G residues confirming the earlier observations that the G-U wobble base pair at the bottom of the ribozyme's recognition segment is strongly preferred (*23*). Moreover, there is no G in position 4 of the targeted sequences, which supports the earlier observations that its presence in this position might be detrimental to cleavage. Reduced cleavage has been observed for short oligonucleotide substrates (*24*), and the most possible sites cleaved by antigenomic ribozyme in HDAg mRNA had no G in this position (*5*).

Low reactivity of X(+) RNA toward the delta ribozyme library prompted us to see whether this RNA was also poorly accessible for other oligonucleotide-based degradation tools. For mapping of RNA accessibility oligodeoxyribonucleotide libraries and RNase H hydrolysis (*25*) were used. Figure 2C shows autoradiograms of the RNase H cleavage reactions occurring in the presence of four 6-mer DNA libraries. In each library the third nucleotide from the 5′ end was fixed in order to facilitate the correlation of the cleavage sites and the most probable sequences of the oligomers engaged in the formation of RNA−DNA hybrids. The cleavages induced by RNase H are displayed in the X(+) RNA secondary structure model showing that several oligodeoxyribonucleotides were able to bind effectively to this RNA, mostly in the hairpin regions: *SL3*, *SL2b* and *SL2a* (Figure 2C). These data contradict our earlier observation of only a few cleavages found with the delta ribozyme library, which clearly suggests that factors other than simple accessibility for hybridization are responsible for low reactivity of X(+) RNA toward ribozyme cleavage.

Yeast $tRNA^{Phe}$ was also subjected to screening for sites accessible for cleavage with the delta ribozyme library. Cleavages were found at G15 and G19 in the D loop region and at U33 in the anticodon loop region (Figure 3A). Their relative intensities were clearly different, and the cleavage at G15 was the strongest, amounting to 1.5% of the input RNA. Unexpectedly, cleavage at this site implies the formation of a D-U base pair immediately adjacent to the cleavage site. It is unclear how such interaction could influence the delta ribozyme performance although the presence of standard Py-Py base pairs at this position has been shown to result in low activity of the genomic variant (*26*). In order to predict the relative efficacy of antisense oligomers or ribozymes, the RNAstructure computer program can be applied (*27*). The program calculates the overall ΔG binding values relevant for the predicted stability of the oligonucleotide tool−target duplex and the competition with predicted secondary structure of both the target and the oligonucleotide. However, it has been shown that the experimental efficacy of antisense oligonucleotides better correlates with the oligonucleotide−RNA duplex stability of intramolecular pairing (*28*). In our case the stabilization energy of bimolecular RNA−RNA duplexes consisting of seven base pairs and corresponding to ribozyme cleavage at G15, G19, and U33 is −9.4, −9.1, and −5.6 kcal/mol, respectively. Thus the experimentally observed strongest ribozyme cleavage at G15 correlates with the most favorable energy of the ribozyme−substrate duplex predicted in silico.

Oligodeoxyribonucleotide libraries and RNase H digestion were also used for mapping of the accessible sites for hybridization on the yeast $tRNA^{Phe}$ in vitro transcript. Figure 3B shows autoradiograms of RNase H cleavage reactions, and the cleavage sites are displayed in the tRNA secondary structure model. It turned out that several DNA oligomers were able to bind effectively to this RNA, inducing RNase H cleavages. The most efficient cleavages occurred at U6 in the acceptor stem, at G19-A21 in the D-loop region, and at G46 in the extra loop of tRNA. Weaker cleavages showed that oligonucleotides were also able to bind to the anticodon and TΨC loops. The data exemplify the crucial role of RNA structural features in the binding of antisense oligomers; similarly, as it has been observed earlier for the genomic and antigenomic delta ribozymes (*25*). Not only are the RNA loops accessible for hybridization of complementary oligonucleotides; oligomers can also partially penetrate some double-stranded regions. Moreover, there are indications that some RNase H cleavages can occur despite the presence of base pair mismatches in the corresponding DNA−RNA heteroduplexes. Cleavages that do not follow the assumed model of RNase H action have been also observed while using the same approach to mapping of the genomic and antigenomic delta ribozymes (*25*).

Cleavage of Structured RNAs by Site-Specific Ribozymes. On the basis of the results of using the delta ribozyme library we synthesized several specifically acting ribozymes. They were used in cleavage reactions at 1 μM concentration, ensuring large ribozyme excess over the analyzed RNA targets. In the case of X(+) RNA it turned out that ribozymes R35 and R46 cleaved the target at the predicted sites but with very modest efficacy at the level of 1% after 6 h (Figure 2A). Moreover, there were no obvious differences in cleavage efficacy despite different stabilization energy of the corresponding bimolecular seven base pair substrate−ribozyme duplexes, which is −5.2 and −10.1 kcal/mol for the R35

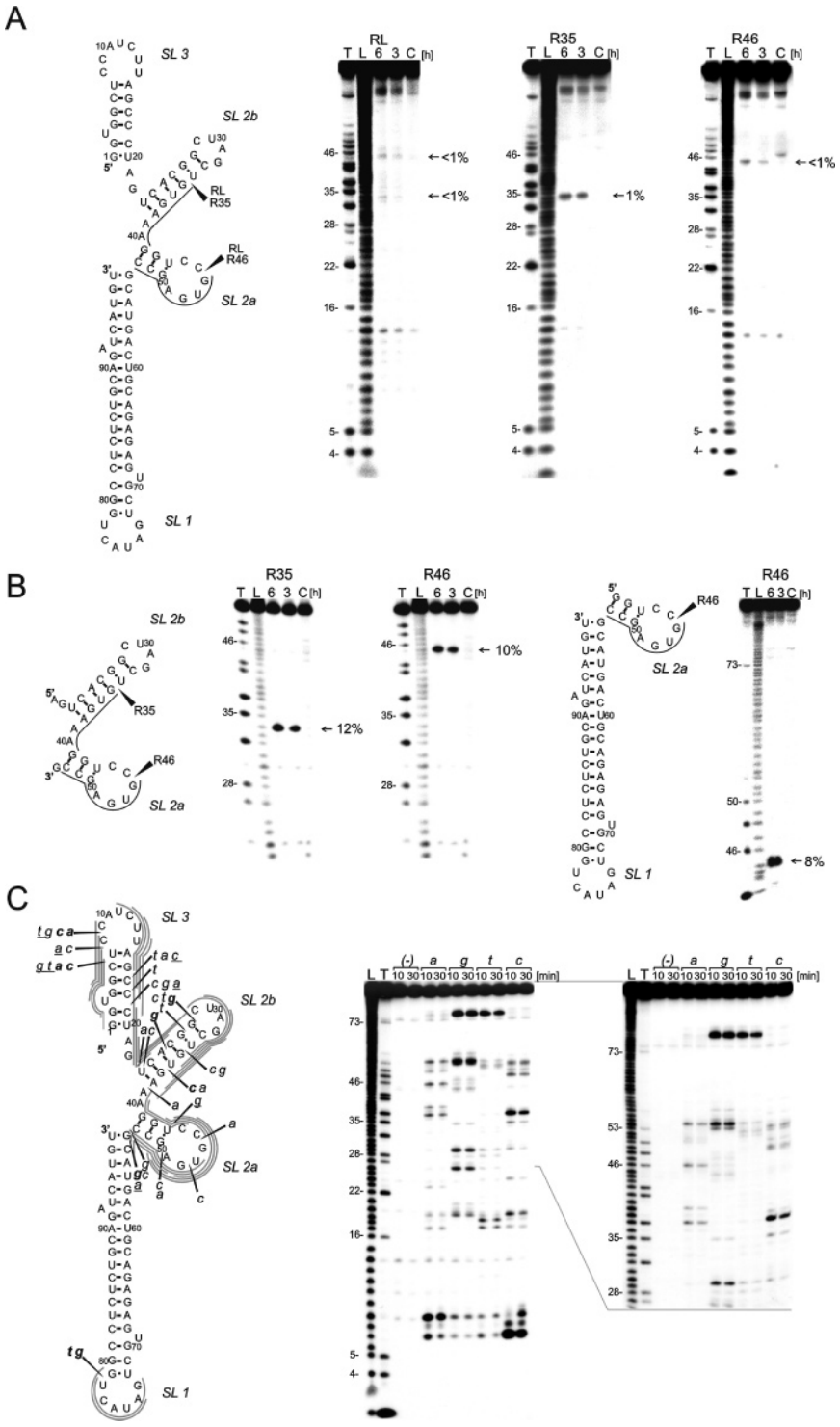

FIGURE 2: Susceptibility of X(+) RNA to cleavage with delta ribozymes and its accessibility for hybridization of complementary oligonucleotides. (A) The autoradiograms on the right show the susceptibility of X(+) RNA to ribozyme cleavage in the presence of ribozyme library RL and sequence-specific ribozymes R35 and R46. The cleavage reactions were performed for 3 and 6 h at 37 °C. Lanes: C, reaction control was incubated for 6 h at 37 °C; L, formamide ladder; T, limited hydrolysis by RNase T1. Some of the guanine residues are shown on the autoradiograms on the left, and cleavage extents are indicated in percentages. On the left, cleavage sites are marked with filled triangles in the X(+) RNA secondary structure. Lines along the structure denote ribozyme recognition sequences. (B) Susceptibility of X(+) RNA subfragments, SL2a/SL2b (left) and SL1/SL2a (right), to cleavage with delta ribozymes R35 and R46. The description of symbols is analogous to that shown in panel A. (C) Mapping of accessible sites on the X(+) RNA with RNase H and four semirandom oligonucleotide libraries *a*, *g*, *t*, and *c* of a general sequence: 5′-nnxnnn-3′ where x represents a, g, c, or t deoxyribonucleotides, respectively, and n denotes their random mixture. On the right, autoradiograms of RNA fragments showing cleavage of the X(+) RNA with RNase H in the presence of oligonucleotide libraries are shown. 5′-^{32}P-end-labeled RNA was used, and short and long runs of the gel are presented in the figure. Lanes: L, formamide ladder; T, limited hydrolysis by RNase T1. Some of the guanine residues are numbered on the left sides of the autoradiograms. Cleavage sites are displayed in the X(+) RNA secondary structure model. Cleavages occurring in the presence of libraries *a*, *c*, *g*, and *t* are marked by filled triangles. Gray lines along the RNA sequences show the most probable positions of oligonucleotides hybridizing to the RNA targets (see ref *25*). Bold letters in italics show exceptionally strong cleavages, and underlined letters denote cleavages to which the corresponding oligonucleotides could not be assigned.

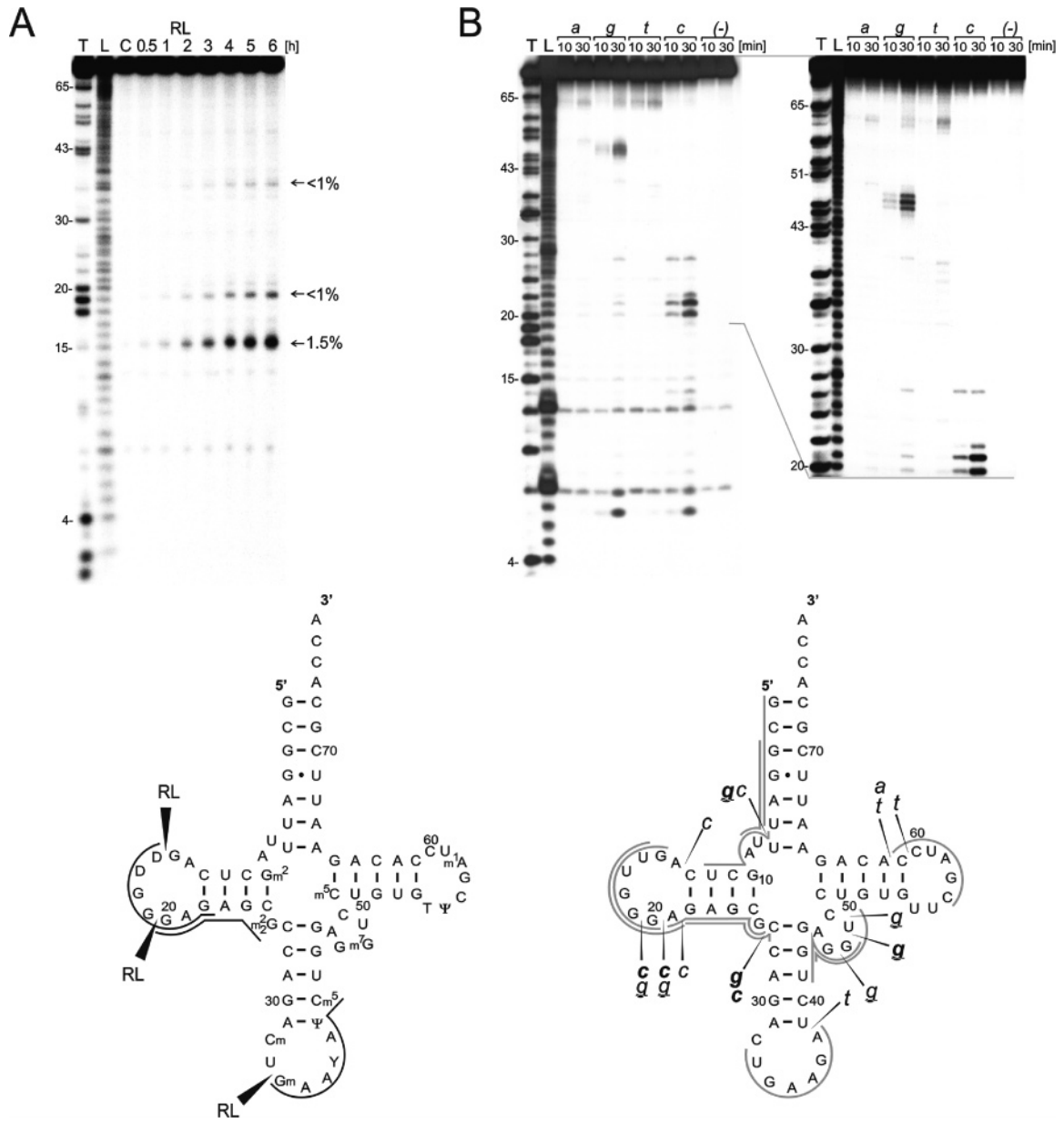

FIGURE 3: Comparison of susceptibility of yeast tRNA^{Phe} to cleavage with delta ribozymes and accessibility for hybridization of complementary oligonucleotides. (A) The cleavage reaction of 5′-^{32}P-end-labeled yeast tRNA^{Phe} was carried out in the presence of ribozyme library RL for up to 6 h at 37 °C. Lanes: L, formamide ladder; T, limited hydrolysis by RNase T1. Guanine residues are numbered on the left. Cleavage sites are marked in the tRNA secondary structure model with filled triangles. Lines along the structure denote ribozyme recognition sequences. (B) Mapping of accessible sites on the yeast tRNA^{Phe} in vitro transcript with RNase H and four semirandom oligonucleotide libraries *a*, *g*, *t*, and *c*. Autoradiograms of RNA fragments showing cleavage of 5′-^{32}P-end-labeled RNA with RNase H in the presence of oligonucleotide libraries are shown. Short and long runs of the gel are presented. Lanes: L, formamide ladder; T, limited hydrolysis by RNase T1. Guanine residues are numbered on the left. Cleavage sites occurring in the presence of libraries *a*, *c*, *g*, and *t* are marked by filled triangles on the tRNA secondary structure model. Gray lines along the RNA sequence show the most probable positions of oligonucleotides hybridizing to the RNA target (see also the legend to Figure 2C).

and R46 ribozymes, respectively. It might be supposed that low efficiency of cleavages induced in the presence of ribozyme combinatorial libraries was a consequence of action of the particular ribozyme variants under subsaturating conditions. This assumption was not correct for the studied RNA targets since low cleavage efficiencies were also observed with a large excess of specifically acting ribozyme variants. Since the targeted regions were fairly susceptible to binding of short oligonucleotides and RNase H digestion, thus in that case accessibility did not seem to be the major factor limiting efficacy of ribozyme cleavage.

In order to find out to what extent the spatial folding of X(+) RNA might influence ribozyme cleavage, two subfragments of this molecule were synthesized (Figure 2B). The fragment SL2a/SL2b spans nucleotides A21−G53, and the mfold computer program predicts that it folds into two hairpin motifs with the total stabilization energy of −9.1 kcal/mol and T_m 70.2 °C. The second fragment, SL1/SL2a with a ΔG of −27.9 kcal/mol (Figure 2B), consisted of the very stable hairpin *SL1* and a 12 nucleotide long stretch which formed rather unstable hairpin *SL2a* (the ΔG values of −26.5 and −1.2 kcal/mol were calculated for both isolated hairpin

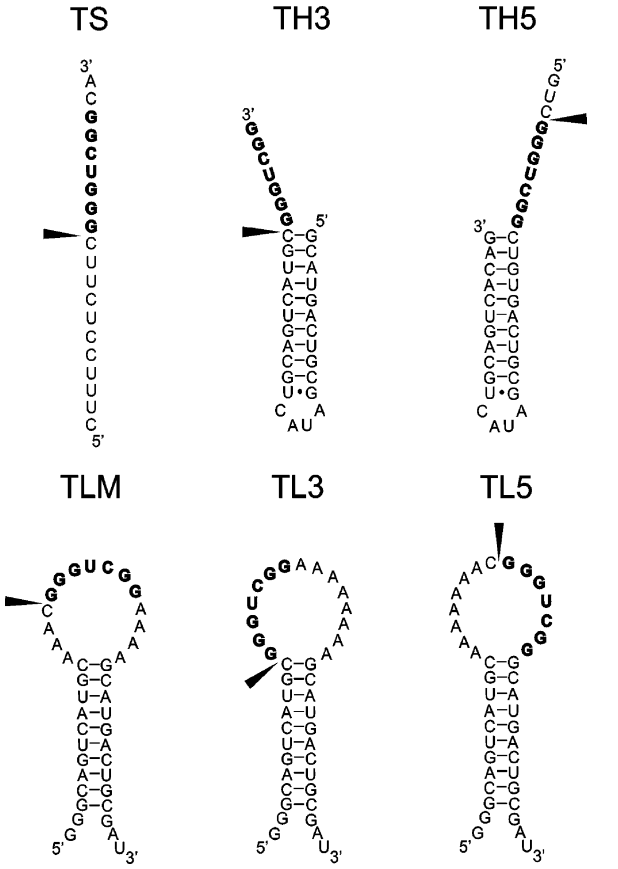

FIGURE 4: Secondary structures of six model RNA substrates with the ribozyme recognition sequence (marked with bold letters) embedded into a different structural context.

motifs, respectively). These two RNA subfragments were subjected to cleavage with ribozymes R35 and R46 used at 1 μM concentration under conditions of single ribozyme turnover. The cleavage extents were substantially higher than those observed with the full-length X(+) RNA but still at the level not exceeding 12% after 6 h (Figure 2B). Again, there was no correlation between the very similar cleavage extents and the different stabilization energies of corresponding seven base pair RNA−RNA duplexes (−5.2 and −10.1 kcal/mol for R35 and R46, respectively).

Ribozyme Cleavage of Model RNA Substrates. In order to gain some more information on how the neighboring structural context of targeted RNA regions might influence their cleavage with the delta ribozyme, we synthesized six model RNA substrates (Figure 4). The substrates contained the same seven nucleotide long stretch 5′-GGGUCGG-3′, which was recognized by the wild-type antigenomic delta ribozyme. In the TS substrate the stretch was embedded into an RNA 20-mer which did not form any stable secondary structure. The other substrates were purposefully designed as RNA hairpins (Figure 4). Their secondary structures were confirmed in silico by the RNAstructure computer program as well as experimentally by the Pb^{2+}-induced cleavage method (*29*) (data not shown). In order to monitor the efficiency of formation of ribozyme−substrate complexes, a catalytically inactive variant of the ribozyme with the single mutation C76G was applied. This variant was used at 1 μM concentration to bind trace amounts of ^{32}P-labeled substrates, TH3, TH5, and TLM under the same ionic conditions, which were applied in ribozyme cleavage reactions. Subsequently,

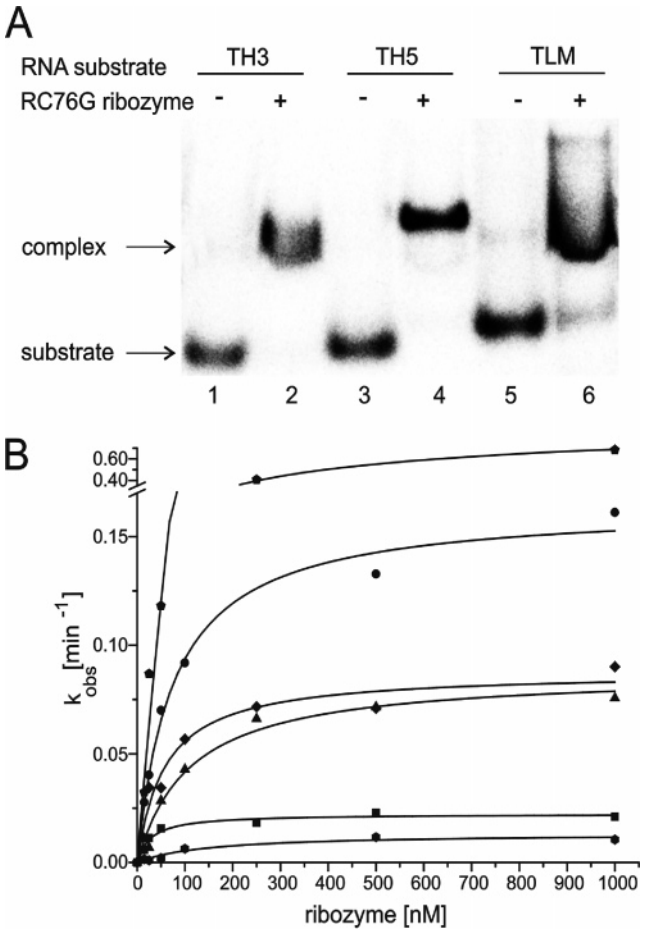

FIGURE 5: Analysis of ribozyme−substrate complexes on nondenaturing polyacrylamide gels and kinetics of ribozyme cleavage. (A) Electrophoretic separation of the TH3, TH5, and TLM substrates and their complexes with catalytically inactive delta ribozyme RC76G on 10% polyacrylamide gel under nondenaturing conditions. 5′-^{32}P-end-labeled RNA substrates with a 100-fold excess of unlabeled ribozyme were hybridized under conditions specified in the Experimental Procedures section. (B) Cleavage kinetics of six model RNA substrates with the wild-type delta ribozyme. The ribozyme was used at concentrations in the range of 15−1000 mM. First-order rate constants k_{obs} were calculated from data fitted to a single exponential equation, $[P]_t = [EP](1 - e^{-k_{obs}t})$, where EP are the reaction end points. Filled symbols in the graph denote k_{obs} values determined for the following substrates: TS (pentagons), TH3 (circles), TH5 (diamonds), TL3 (hexagons), TLM (squares), and TL5 (triangles).

the samples were subjected to electrophoresis in native polyacrylamide gels (Figure 5A). It turned out that essentially all of the substrate molecules were complexed with the delta ribozyme under such conditions.

The susceptibility of the six model RNA substrates to ribozyme cleavage was tested using the wild-type antigenomic delta ribozyme. Preliminary experiments showed that both reaction rates and cleavage extents after 60 min greatly varied depending on the structural context in which the targeted sequence was embedded. These differences were characterized in detail in further studies. The k_{obs} values were determined using ca. 2 nM RNA substrates and the following concentrations of the ribozyme: 15, 25, 50, 100, 250, 500, and 1000 nM. The maximum first-order rate constants at the saturating ribozyme concentration, k_2, and the concentrations of ribozyme at which the reaction rates were half-maximal, K_M, were calculated for each RNA substrate

Table 1: Michaelis−Menten Parameters for Delta Ribozyme Cleavage

RNA substrate	k_2 (min^{-1})	K_M (nM)	k_2/K_M (min^{-1} M^{-1}) × 10^6	Fr_{60min} (%)
TS	0.91 ± 0.03	326 ± 30	2.8 ± 0.3	87
TH3	0.16 ± 0.01	75 ± 9	2.2 ± 0.4	92
TH5	0.088 ± 0.005	58 ± 15	1.7 ± 0.5	32
TL5	0.087 ± 0.005	110 ± 21	0.83 ± 0.20	86
TLM	0.022 ± 0.001[a]	28 ± 5	0.81 ± 0.18	63
TL3	0.021 ± 0.002[a]	371 ± 70	0.06 ± 0.02	60

[a] To determine the cleavage rate for the TLM and TL3 substrates, reaction aliquots were taken at specified time points and quantified after electrophoretic separation, and subsequently the logarithm of the percent RNA remaining was plotted as a function of time. The negative slope of the least-squares plot yielded the cleavage rate.

(Figure 5B and Table 1). The k_2 and K_M parameters gave second-order rate constants k_2/K_M. At saturating ribozyme concentration the TS, TH3, and TL5 substrates were cleaved to ca. 90% after 60 min. For TLM and TL3 the cleavage extents were still high, reaching the level of 60%. Only the TH5 substrate was cleaved reproducibly to a smaller extent (ca. 30%), but the reason for that was unclear. The k_2 of 0.91 min^{-1} obtained for TS is consistent with similar values that have been determined by Shih and Been for another antigenomic ribozyme construct and a series of short oligonucleotide substrates (*30*). In the cited studies the corresponding K_M values grew along with the length of the sequence preceding the cleavage site, and for the eight nucleotide stretch it was 225 nM. Thus the value of 300 nM obtained in this work for TS with 11 residues which are cleaved off seems to be very reasonable. For the other substrates the K_M values were in the range of 30−400 mM; thus they were similar to those determined by Shih and Been for their substrates (*30*).

DISCUSSION

Sites Susceptible to Ribozyme Cleavage Are Much Less Frequent Than Those Accessible for Binding of Antisense Oligonucleotides. Scanning of RNA-accessible sites using combinatorial libraries of ribozymes has been shown to be more effective and rapid in comparison with the traditional sequence-selected procedure (*6*, *31*−*33*). Libraries of the delta ribozyme are particularly useful for the purpose of mapping the susceptibility of highly structured RNA molecules to ribozyme cleavage since the randomized region responsible for ribozyme−target interaction consists of only seven base pairs (Figure 1). In the case of other ribozymes larger double-stranded recognition segments are required. It results in more differentiated libraries in which the particular variants are present in a relatively small number of copies. Despite the "high mapping potency" of delta ribozymes only two ribozyme-induced cleavage sites, at U34 and C45, were found in an oligonucleotide that corresponded to region X of HCV viral RNA (Figure 2A). The cleavage sites are located in the region that has been shown to fold into two small hairpins, which may further form a pseudoknot structure (*21*).

It has been reported earlier (*34*) that out of three DNAzymes of type 10-23 designed to attack the X region between nucleotides A21 and G53, only the one with substrate binding arms complementary to nucleotides A39−G53 exhibited a detectable cleavage activity at the predicted G46 site. The other two DNAzymes were inactive despite the accessibility of the attacking regions for hybridization of DNA 15-mers and RNase H digestion (*34*). The results described in this report with the use of semirandom libraries of DNA 6-mers and RNase H (*25*) also show that the region consisting of two hairpins, *2a* and *2b*, is accessible for hybridization of short complementary oligonucleotides (Figure 2C). Thus identification in this region of only two cleavages induced in the presence of the delta ribozyme library is rather unexpected. On the other hand, it is in line with some earlier observations showing that in longer RNA molecules relatively few ribozyme cleavages are induced despite their accessibility for hybridization of complementary oligonucleotides. This implies in practice that the results of the RNA accessibility studies derived from the ribonuclease H mapping method should be applied very cautiously to planning the sites susceptible to ribozyme attack.

Using the library of delta ribozyme we identified three sites in yeast $tRNA^{Phe}$ susceptible to ribozyme cleavage, two cleavages in the D-loop and one in the anticodon loop (Figure 3A). The first two cleavages are located within the regions that have been determined by Mir and Southern by the oligonucleotide microarray method as able to effectively hybridize RNA 8- and 12-mers (*35*). Their data correspond very nicely with the results of RNase H mapping experiments described in this report. Both methods identified additional tRNA regions accessible for hybridization, in particular the anticodon loop, the extra loop, and the TΨC arm (*35*; Figure 3B). Out of all these regions cleavage was induced only in the anticodon loop in the presence of the delta ribozyme library.

Following determination of the regions susceptible to cleavage on the X(+) RNA and yeast $tRNA^{Phe}$ several sequence-specific ribozymes were synthesized. It turned out that the ribozymes cleaved the targets precisely at the predicted sites, albeit with unexpectedly modest efficacy. In the X(+) RNA similar cleavage extents at the level of 1% were observed with ribozymes R35 and R46 at two targeted sequences, 5′-GUGAAAG-3′ and 5′-GUGAGCC-3′, respectively (Figure 2A), despite the substantially different stability of the double-stranded recognition segments amounting to −5.2 and −10.1 kcal/mol for the corresponding RNA−RNA interactions in substrate−ribozyme complexes. In the case of the subfragment of X(+) RNA, SL1/SL2a, the R46 ribozyme was targeted to an RNA stretch which formed a thermodynamically very unstable hairpin motif. But even in this case cleavage occurred with relatively low efficiency, suggesting that the directly adjacent double-stranded stem *SL1* might be detrimental to ribozyme catalysis. Clearly, cleavage efficiency depended not only on the ability of the targeted sequences to bind ribozymes but also on the structural context in which these targets were embedded within larger RNA molecules.

Cleavage of Single-Stranded RNA Is Strongly Influenced by the Surrounding Structural Context. In order to determine to what extent the structural context might influence ribozyme cleavage, six model RNA substrates were assayed (Figure 4). Each substrate contained the same single-stranded RNA sequence that should be recognized and cleaved by the wild-type delta ribozyme. The first substrate was a 20

nucleotide long unstructured oligoribonucleotide in which the ribozyme cleavage site was preceded by 11 nucleotides. In the next two substrates the targeted sequence was immediately adjacent to a double-stranded helical stem, at its 3′ and 5′ side in both substrates, respectively. In the last three substrates the recognized stretch was placed in a large apical loop being either directly adjacent to the double-stranded stem or located centrally in the loop. In all of these RNA substrates one could expect that the ribozyme should bind effectively to the predicted sites of the targets. The calculated energy of the corresponding bimolecular RNA−RNA segment is −11.1 kcal/mol. The cleavage reactions were performed under single turnover conditions with large ribozyme excess. Under such conditions essentially all of the substrate molecules were bound to the ribozyme as it was confirmed by electrophoresis in native conditions of complexes consisting of catalytically inactive ribozyme mutant C76G and substrates TL5, TLM, and TL3 (Figure 5A).

Unexpectedly, the ribozyme cleaved the model RNA hairpins with differentiated rates, which were much slower than that observed for a short unstructured oligoribonucleotide. The k_2 values were in the range from 0.91 to 0.021 min^{-1}; thus they differed almost 50-fold (Figure 5B and Table 1). The highest k_2 of 0.91 min^{-1} was obtained for the TS substrate. This value was comparable to those in the range of 0.35−1 min^{-1}, which have been determined by other authors for five oligonucleotide substrates with one to five nucleotides preceding the cleavage site (*30*). In other studies with short substrates bearing single mutations within the four nucleotide long region 5′ to the cleavage site (positions −1 to −4), it has been shown that nucleotides in positions −1 and −2 exerted the most pronounced influence on cleavage efficiency (*36*). For the substrates with only one nucleotide 5′ to the cleavage site the presence of G was most detrimental. The corresponding k_2 value was 18-fold lower than that for the substrate with U and 8-fold for the substrate with C in this position. In position −2, A or G seemed to be preferred. Changes in positions −3 and −4 resulted in less than 2-fold differences in k_2 values (*36*). Taking into account the above data and the sequence of the first few nucleotides that precede the cleavage sites in the RNA hairpin substrates used in our studies, we expected cleavage rates similar to that characteristic of the TS oligonucleotide. However, the k_2 values were lower by a factor of 6 for TH3 and more than 40 for TLM and TL3 (Table 1). Importantly, these differences were far more pronounced than those derived from nonoptimal sequences that immediately preceded the cleavage site in short oligoribonucleotides (*36*). Clearly, the susceptibility of single-stranded RNA targets toward delta ribozyme cleavage depends on their placement in a larger context of the RNA secondary structure. The cleavage reactions slow down when ordered RNA motifs are immediately adjacent either at their 3′ or at their 5′ sides, which is the case of substrates TH3 and TH5. The cleavage rates are even slower in the case of targets constrained in apical RNA loops, as in substrates TL5, TLM, and TL3 (Table 1).

Implications for the Ribozyme Cleavage Mechanism and Practical Ribozyme Applications. Recent crystallographic studies of a catalytically inactive mutant of the genomic delta ribozyme (*37*) have shown that the substrate RNA strand preceding the cleavage site makes a sharp turn between the G1 and U(−1) bases, packing the substrate strand into the P1 major groove and possibly destabilizing the ribozyme ground state. Furthermore, the G1 and U(−1) nucleotides are involved in coordination of a catalytically critical divalent metal ion, which is ejected from the active site after cleavage. Importantly, these observations suggest that a conformational switch might control delta ribozyme catalysis (*37*).

The minimal kinetic pathway of *trans*-acting delta ribozyme cleavage assumes that after formation of the ribozyme−substrate complex (RzS) this complex is rearranged to the active complex (RzS′), which subsequently undergoes the chemical cleavage reaction (*1*, *38*, *39*). The initially formed complex might also be in equilibrium with the nonproductive complex (RzS*) that is off on the reaction pathway. Previous kinetic analyses have suggested that conformational rearrangement from RzS to RzS′ is a limiting step in the kinetic pathway. Moreover, it has been proposed that further conformational changes of the complex take place during the chemical step of the reaction (*1*, *38*, *39*). Recently published data have documented the occurrence of large conformational changes during delta ribozyme catalysis (*40*−*44*). It is conceivable that in *trans*-acting ribozyme such changes would require substantial flexibility of the substrate RNA strand, possibly not only in the region directly interacting with the ribozyme but in a wider structural context. Indeed, in this work we showed that double-stranded segments immediately adjacent to the ribozyme's recognition sequence located at the RNA terminus are detrimental to cleavage. On the other hand, we have shown earlier that the same seven nucleotide long stretch attached to the 3′ end of yeast $tRNA^{Phe}$ can be effectively cleaved off with kinetics similar to a short oligonucleotide substrate (*14*). In that case, however, the tRNA 3′ terminus 73-ACCA-76 separates the stretch from the double-stranded segment of the acceptor stem.

It has been observed that ribozymes cleave long RNA molecules much less effectively than short oligonucleotide substrates (*5*, *10*, *33*). The observed differences are at least 30−100-fold, and they depend on the ribozymes and cleavage systems used (*5*, *8*). Earlier explanations have suggested that low accessibility of the targeted regions for ribozyme hybridization and the thermodynamics of the enzyme−substrate interactions are responsible for these differences (*10*, *45*). The ability of RNA substrates to form active ribozyme−target complexes has also been supposed to be of importance (*6*); however, no closer evaluation of such effects has been made. In this work we showed that despite full accessibility of the targeted regions for hybridization their cleavage with the delta ribozyme might be up to 50-fold slower than with a short oligonucleotide substrate (Figure 5). Structural constraints imposed on the targeted sequence in a large RNA molecule seem to be responsible for this effect. Restricted possibilities of conformational transitions which are necessary to occur on the cleavage reaction trajectory result in slower ribozyme cleavage in comparison to that observed with a short unstructured oligomer. It has been shown that changing the *cis*-acting antigenomic delta ribozyme to its *trans*-acting form results in a ca. 50 times lower cleavage rate (*1*, *22*). Furthermore, the same *trans*-acting ribozyme may cleave up to 50-fold more slowly when targeting an accessible but structurally

constrained target sequence (this work). It might be one of the reasons for the lack of relationship between the activities of ribozymes in cultured cells and the kinetic parameters of their respective chemical cleavage reactions in vitro (*10*). In light of the results described in this work one may also speculate that ribozymes seem to be less attractive than other oligonucleotide-based tools to attack highly structured RNA targets. Although our conclusions concern functioning of the delta ribozyme, they are likely valid for other ribozymes. Conformational switches have also been proposed to occur during catalysis of the hammerhead (*46*) and hairpin (*47*) ribozymes. However, it still remains to be determined to what extent the conformational constraints, which are characteristic features of highly structured RNA targets, may influence cleavage abilities of these nucleic acid-based tools.

ACKNOWLEDGMENT

We thank Barbara Smólska for expert technical assistance and Agnieszka Wichłacz and Jan Wrzesinski for critical review of the manuscript.

REFERENCES

1. Shih, I. H., and Been, M. D. (2002) Catalytic strategies of the hepatitis delta virus ribozymes, *Annu. Rev. Biochem. 71*, 887−917.
2. Wadkins, T. S., and Been, M. D. (2002) Ribozyme activity in the genomic and antigenomic RNA strands of hepatitis delta virus, *Cell. Mol. Life Sci. 59*, 112−125.
3. Bergeron, L. J., Ouellet, J., and Perreault, J. P. (2003) Ribozyme-based gene-inactivation systems require a fine comprehension of their substrate specificities; the case of delta ribozyme, *Curr. Med. Chem. 10*, 2589−2597.
4. Levesque, D., Choufani, S., and Perreault, J. P. (2002) Delta ribozyme benefits from a good stability *in vitro* that becomes outstanding *in vivo*, *RNA 8*, 464−477.
5. Roy, G., Ananvoranich, S., and Perreault, J. P. (1999) Delta ribozyme has the ability to cleave *in trans* an mRNA, *Nucleic Acids Res. 15*, 942−948.
6. Bergeron, L. J., and Perreault, J. P. (2002) Development and comparison of procedures for the selection of delta ribozyme cleavage sites within the hepatitis B virus, *Nucleic Acids Res. 1*, 4682−4691.
7. D'Anjou, F., Bergeron, L. J., Larbi, N. B., Fournier, I., Salzet, M., Perreault, J. P., and Day, R. (2004) Silencing of SPC2 expression using an engineered delta ribozyme in the mouse βTC-3 endocrine cell line, *J. Biol. Chem. 2*, 14232−14239.
8. Al-Anouti, F., and Ananvoranich, S. (2002) Comparative analysis of antisense RNA, double-stranded RNA, and delta ribozyme-mediated gene regulation in *Toxoplasma gondii*, *Antisense Nucleic Acid Drug Dev. 12*, 275−281.
9. Sheng, J., Al-Anouti, F., and Ananvoranich, S. (2004) Engineered delta ribozymes can simultaneously knock down the expression of the genes encoding uracil phosphoribosyltransferase and hypoxanthine-xanthine-guanine phosphoribosyltransferase in *Toxoplasma gondii*, *Int. J. Parasitol. 9*, 253−263.
10. Kato, Y., Kuwabara, T., Warashina, M., Toda, H., and Taira, K. (2001) Relationships between the activities *in vitro* and *in vivo* of various kinds of ribozyme and their intracellular localization in mammalian cells, *J. Biol. Chem. 276*, 15378−15385.
11. Fiola, K., Perreault, J. P., and Cousineau, B. (2006) Gene targeting in the gram-positive bacterium *Lactococcus lactis*, using various delta ribozymes, *Appl. Environ. Microbiol. 72*, 869−879.
12. Yu, Y. C., Mao, Q., Gu, C. H., Li, Q. F., and Wang, Y. M. (2002) Activity of HDV ribozymes to *trans*-cleave HCV RNA, *World J. Gastroenterol. 8*, 694−698.
13. Schurer, H., Lang, K., Schuster, J., and Morl, M. (2002) A universal method to produce *in vitro* transcripts with homogeneous 3′ ends, *Nucleic Acids Res. 30*, e56.
14. Wichłacz, A., Łęgiewicz, M., and Ciesiołka, J. (2004) Generating *in vitro* transcripts with homogenous 3′ ends using *trans*-acting antigenomic delta ribozyme, *Nucleic Acids Res. 32*, e39.
15. Cullen, B. R. (2006) Enhancing and confirming the specificity of RNAi experiments, *Nat. Methods 3*, 677−681.
16. Rossi, J. J. (2006) RNAi as a treatment for HIV-1 infection, *BioTechniques Suppl.*, 25−29.
17. Gitlin, L., Karelsky, S., and Andino, R. (2002) Short interfering RNA confers intracellular antiviral immunity in human cells, *Nature 418*, 430−434.
18. Boden, D., Pusch, O., Lee, F., Tucker, L., and Ramratnam, B. (2003) Human immunodeficiency virus type 1 escape from RNA interference, *J. Virol. 77*, 11531−11535.
19. Yokota, T., Sakamoto, N., Enomoto, N., Tanabe, Y., Miyagishi, M., Maekawa, S., Yi, L., Kurosaki, M., Taira, K., Watanabe, M., and Mizusawa, H. (2003) Inhibition of intracellular hepatitis C virus replication by synthetic and vector-derived small interfering RNAs, *EMBO Rep. 4*, 602−608.
20. Wilson, J. A., and Richardson, C. D. (2006) Future promise of siRNA and other nucleic acid based therapeutics for the treatment of chronic HCV, *Infect. Disord. Drug Targets 6*, 43−56.
21. Dutkiewicz, M., and Ciesiołka, J. (2005) Structural characterization of the highly conserved 98-base sequence at the 3′ end of HCV RNA genome and the complementary sequence located at the 5′ end of the replicative viral strand, *Nucleic Acids Res. 33*, 693−703.
22. Wrzesiński, J., Łęgiewicz, M., Smólska, B., and Ciesiołka, J. (2001) Catalytic cleavage of *cis*- and *trans*-acting antigenomic *delta* ribozymes in the presence of various divalent metal ions, *Nucleic Acids Res. 29*, 4482−4492.
23. Nishikawa, F., Roy, M., Fauzi, H., and Nishikawa, S. (1999) Detailed analysis of stem I and its 5′ and 3′ neighbor regions in the *trans*-acting HDV ribozyme, *Nucleic Acids Res. 27*, 403−410.
24. Ananvoranich, S., Lafontaine, D. A., and Perreault, J. P. (1999) Mutational analysis of the antigenomic *trans*-acting delta ribozyme: the alterations of the middle nucleotides located on the P1 stem, *Nucleic Acids Res. 27*, 1473−1479.
25. Wrzesiński, J., Łęgiewicz, M., and Ciesiołka, J. (2000) Mapping of accessible sites for oligonucleotide hybridization on hepatitis delta virus ribozymes, *Nucleic Acids Res. 28*, 1785−1793.
26. Nishikawa, F., Fauzi, H., and Nishikawa, S. (1997) Detailed analysis of base preferences at the cleavage site of a *trans*-acting HDV ribozyme: a mutation that changes cleavage site specificity, *Nucleic Acids Res. 25*, 1605−1610.
27. Mathews, D. H. (2005) Predicting a set of minimal free energy RNA secondary structures common to two sequences, *Bioinformatics 21*, 2246−2253.
28. Matveeva, O. V., Mathews, D. H., Tsodikov, A. D., Shabalina, S. A., Gesteland, R. F., Atkins, J. F., and Freier, S. M. (2003) Thermodynamic criteria for high hit rate antisense oligonucleotide design, *Nucleic Acids Res. 31*, 4989−4994.
29. Kirsebom, L. A., and Ciesiołka, J. (2005) Pb^{+2}-induced cleavage of RNA, in *Handbook of RNA Biochemistry* (Westhof, E., Bindereif, A., Schön, A., and Hartmann, R. K., Eds.) pp 214−228, Wiley-VCH Verlag, Weinheim, Germany.
30. Shih, I., and Been, M. D. (2001) Energetic contribution of non-essential 5′ sequence to catalysis in a hepatitis delta virus ribozyme, *EMBO J. 20*, 4884−4891.
31. Campbell, T. B., and Cech, T. R. (1995) Identification of ribozymes within a ribozyme library that efficiently cleave a long substrate RNA, *RNA 1*, 598−609.
32. Lieber, A., and Strauss, M. (1995) Selection of efficient cleavage sites in target RNAs by using a ribozyme expression library, *Mol. Cell. Biol. 15*, 540−551.
33. Yu, Q., Pecchia, D. B., Kingsley, S. L., Heckman, J. E., and Burke, J. M. (1998) Cleavage of highly structured viral RNA molecules by combinatorial libraries of hairpin ribozymes, *J. Biol. Chem. 273*, 23524−23533.
34. Smith, R. M., Walton, C. M., Wu, C. H., and Wu, G. Y. (2002) Secondary structure and hybridization accessibility of hepatitis C virus 3′-terminal sequences, *J. Virol. 76*, 9563−9574.
35. Mir, K. U., and Southern, E. M. (1999) Determining the influence of structure on hybridization using oligonucleotide arrays, *Nat. Biotechnol. 17*, 788−792.
36. Deschenes, P., Lafontaine, D. A., Charland, S., and Perreault, J. P. (2000) Nucleotides −1 to −4 of hepatitis delta ribozyme substrate increase the specificity of ribozyme cleavage, *Antisense Nucleic Acid Drug Dev. 10*, 53−61.

37. Ke, A., Zhou, K., Ding, F., Cate, J. H., and Doudna, J. A. (2004) A conformational switch controls hepatitis delta virus ribozyme catalysis, *Nature 429*, 201−205.
38. Mercure, S., Lafontaine, D. A., Ananvoranich, S., and Perreault, J. P. (1998) Kinetic analysis of delta ribozyme cleavage, *Biochemistry 37*, 16975−16982.
39. Shih, I., and Been, M. D. (2000) Kinetic scheme for intermolecular RNA cleavage by a ribozyme derived from hepatitis delta virus RNA, *Biochemistry 39*, 9055−9066.
40. Pereira, M. J., Harris, D. A., Rueda, D., and Walter, N. G. (2002) Reaction pathway of the *trans*-acting hepatitis delta virus ribozyme: A conformational change accompanies catalysis, *Biochemistry 41*, 730−740.
41. Harris, D. A., Rueda, D., and Walter, N. G. (2002) Local conformational changes in the *trans*-acting hepatitis delta virus ribozyme accompany catalysis, *Biochemistry 41*, 12051−12061.
42. Tanaka, Y., Tagaya, M., Hori, T., Sakamoto, T., Kurihara, Y., Katahira, M., and Uesugi, S. (2002) Cleavage reaction of HDV ribozymes in the presence of Mg^{2+} is accompanied by a conformational change, *Genes Cells 7*, 567−579.
43. Harris, D. A., Tinsley, R. A., and Walter, N. G. (2004) Terbium-mediated footprinting probes a catalytic conformational switch in the antigenomic hepatitis delta virus ribozyme, *J. Mol. Biol. 341*, 389−403.
44. Gondert, M. E., Tinsley, R. A., Rueda, D., and Walter, N. G. (2006) Catalytic core structure of the *trans*-acting HDV ribozyme is subtly influenced by sequence variation outside the core, *Biochemistry 45*, 7563−7573.
45. Cairns, M. J., Hopkins, T. M., Witherington, C., Wang, L., and Sun, L. Q. (1999) Target site selection for an RNA-cleaving catalytic DNA, *Nat. Biotechnol. 17*, 480−486.
46. Dunham, C. M., Murray, J. B., and Scott, W. G. (2003) A helical twist-induced conformational switch activates cleavage in the hammerhead ribozyme, *J. Mol. Biol. 332*, 327−336.
47. Zhuang, X., Kim, H., Pereira, M. J., Babcock, H. P., Walter, N. G., and Chu, S. (2002) Correlating structural dynamics and function in single ribozyme molecules, *Science 296*, 1473−1476.

BI6024287